Dastpak, Arman; Vergara Lourencon, Tainise; Balakshin, Mikhail; Hashmi, Farhan; Lundström, Mari; Wilson, Benjamin P.

Solubility study of lignin in industrial organic solvents and investigation of electrochemical properties of spray-coated solutions

Published in:
Industrial Crops and Products

DOI:
10.1016/j.indcrop.2020.112310

Published: 01/06/2020

Document Version
Publisher's PDF, also known as Version of record

Please cite the original version:
Dastpak, A., Vergara Lourencon, T., Balakshin, M., Hashmi, F., Lundström, M., & Wilson, B. P. (2020). Solubility study of lignin in industrial organic solvents and investigation of electrochemical properties of spray-coated solutions. *Industrial Crops and Products*, *148*, Article 112310. https://doi.org/10.1016/j.indcrop.2020.112310

Industrial Crops & Products 148 (2020) 112310

Contents lists available at ScienceDirect

Industrial Crops & Products

journal homepage: www.elsevier.com/locate/indcrop

Solubility study of lignin in industrial organic solvents and investigation of electrochemical properties of spray-coated solutions

Arman Dastpak[a], Tainise V. Lourençon[b], Mikhail Balakshin[b], Syed Farhan Hashmi[b], Mari Lundström[a], Benjamin P. Wilson[a],*

[a] Hydrometallurgy and Corrosion, Department of Chemical and Metallurgical Engineering (CMET), Aalto University, P.O. Box 16200, FI-00076 Aalto, Espoo, Finland
[b] Department of Bioproducts and Biosystems (Bio^2), School of Chemical Engineering, Aalto University, P.O. Box 16300, FI-00076 Aalto, Espoo, Finland

ARTICLE INFO

Keywords:
Lignin
Solubility
Organic solvent
Sustainable coatings
Corrosion protection

ABSTRACT

In the present study, six organic solvents that are commonly used in the paint industry (1-butanol, 1-methoxy-2-propanol, 2-propanol, butyl acetate, propylene glycol monomethyl ether acetate, and diethylene glycol monobutyl ether) were tested for their ability to dissolve two distinct lignins: an industrial kraft lignin (KL) and a pilot-scale organosolv lignin (OL). Among the solvents investigated, 1-methoxy-2 propanol (Dowanol™ PM, DPM) and diethylene glycol monobutyl ether (Butyl Carbitol™, BC) demonstrated high degrees of solubility (> 98 wt. % at 25 °C) that were comparable to the commonly used lignin solvent, dimethyl sulfoxide (DMSO). Lignin coatings were prepared by spray-coating the new lignin-solvent solutions on iron-phosphated steel, prior to investigation of their subsequent morphological and electrochemical performance characteristics. It was found that KL/DPM coatings demonstrate suitable short-term (1 h, 5% NaCl) anticorrosive characteristics with an increased charge transfer resistance (R_{ct}) compared to the bare steel (1.5×10^5 Ω. cm^2 *cf.* 1.9×10^3 Ω. cm^2). However, a prolonged (24 h) immersion resulted in a decrease in R_{ct} values (1.1×10^4 Ω. cm^2), which may indicate that the lignin coating alone is unable to provide long-term protection under these aggressive conditions.

1. Introduction

Lignin is the most abundant aromatic biopolymer on earth (Chen-Loung, 1991; Ralph et al., 2004), and can be recovered in large quantities as a by-product of pulp and paper industries and sugar-based biorefineries (Berlin and Balakshin, 2014; Glasser, 1999; Holladay et al., 2007; Ragauskas et al., 2014). Notwithstanding the established potential of lignin for the development of sustainable industrial products (Fernandes et al., 2013; Lora and Glasser, 2002; Thakur et al., 2014), only a small proportion (≤ 2%) of the 50 million tons of lignin isolated from pulping processes is utilized in the production of value-added materials (Upton and Kasko, 2016). Some of the main obstacles for the valorization of lignin include the source-induced variation in fundamental properties and the fact that the lignin isolation process affects the structure and properties of the material (Laurichesse and Avérous, 2014). Consequently, these variations in structure limit the reliable utilization of lignin in up-scaled industrial production processes (Hämäläinen et al., 2018) due to the impact they have on properties like solubility in organic solvents (Melro et al., 2018). Therefore, in the search to develop sustainable functional biopolymers it is important to perform solubility studies with different lignin types in a wide range of organic solvents, including those that are widely utilized in industrial procedures like paint and coatings manufacture.

Solubility behavior of different types of lignin in different organic solvents has been extensively studied in the literature (Cybulska et al., 2012; Giummarella et al., 2016; Melro et al., 2018; Sameni et al., 2017; Schuerch, 1952; Shukry et al., 2008; Xue et al., 2016). In general, the dissolution of polymers initially involves the diffusion of solvent and a consequent disentanglement of polymeric chains (Miller-Chou and Koenig, 2003). Similarly, solubility of lignin in organic solvents is related to the solubility parameter – as determined by Hildebrand's theory – that is based on the contribution of cohesion energy. This cohesion energy can also be studied in more detail using the extended Hansen solubility approach in which the cohesion energy is divided into its constituent parts through the consideration of individual molecular interactions - i.e. dispersion, dipole-dipole, and hydrogen bonding - between the solvent and the solute (Koleske and Hansen, 2009). With regards to lignin, organic solvents with Hildebrand solubility parameters around 22.5 (MPa)$^{1/2}$ are known to be strong solvents for isolated lignin, and the solubility strength of such solvents increases in line

---

* Corresponding author.
E-mail address: ben.wilson@aalto.fi (B.P. Wilson).

https://doi.org/10.1016/j.indcrop.2020.112310
Received 31 October 2019; Received in revised form 2 March 2020; Accepted 4 March 2020

with the hydrogen bonding capability (Schuerch, 1952). Nevertheless, due to the complex nature of lignin structures solubility parameters alone are not sufficient to predict solubility behavior (Evstigneev, 2010; Sameni et al., 2017). For example, factors such as a decrease in lignin's polydispersity and molecular weight (Laurichesse and Avérous, 2014; Sameni et al., 2017) or solvent-related properties like an increase in acid-base interaction capability (Evstigneev, 2010) and the decrease in length of aliphatic hydrocarbon side chains can result in higher levels of lignin solubility (Laurichesse and Avérous, 2014).

As a polymeric macromolecule, lignin offers diverse properties such as antioxidant capabilities (Upton and Kasko, 2016) and corrosion inhibition of metallic surfaces in different media (Abu-Dalo et al., 2013; Akbarzadeh et al., 2011; Hussin et al., 2015b, 2015a; Ren et al., 2008; Shivakumar et al., 2017), which suggest lignin has the potential for utilization in bio-based anticorrosive coatings. Although the positive effect of lignin as an additive for anticorrosive coatings has been investigated previously (Ding et al., 2016; Harb et al., 2015; Rahman et al., 2018; Sakhri et al., 2011), the capabilities of high-content lignin coatings as anticorrosive coatings is still virtually unexplored. To the best knowledge of the authors, only a few studies have investigated utilization of unmodified technical lignin as corrosion resistant coatings and these include organosolv lignin-based coatings on stainless steel (Dastpak et al., 2018), and electropolymerized lignosulfonates for the protection of steel surfaces (Vagin et al., 2006). Consequently, there is still a gap in the understanding of the behavior of technical lignin for use as potential anticorrosive coatings.

As a result, this work investigates the capability of industrial organic solvents commonly used in the paint industry for preparation of sustainable anticorrosive coatings. The structural characteristics of two technical lignins (softwood kraft lignin and hardwood organosolv lignin) and their solubility in industrial organic solvents were investigated. Moreover, anticorrosive lignin coatings with high concentrations of lignin in organic solvents were prepared for iron-phosphated steel and subsequently, the physical and electrochemical properties of the resultant organic coatings were evaluated. The results obtained in this study clearly demonstrate the capability of two widely used industrial organic solvents to dissolve unmodified technical lignin. In addition, the anticorrosive capability of the coatings prepared from technical lignin – without any modification – is demonstrated for iron-phosphated steel surfaces.

2. Experimental

2.1. Materials

Two different types of lignin were used for the dissolution experiments: An industrial grade softwood kraft lignin (KL), BioPiva™ 190 (UPM, Helsinki, Finland) and a pilot-scale hardwood organosolv lignin (OL) (Fraunhofer Center for Chemical-Biotechnological Processes (CBP), Leuna, Germany). Details of the procedure for the isolation of the organosolv lignin from spent liquors have been reported previously (Rossberg et al., 2019). Six types of organic solvents that are utilized in the paint industry were chosen as the test medium and were used without any modifications. The selected solvents were butyl acetate (≥ 99 %), 2-propanol (≥ 99.7 %), propylene glycol monomethyl ether acetate (Dowanol™ PMA, ≥ 99.5 %), 1-methoxy-2-propanol (Dowanol™ PM, ≥ 99.5 %), diethylene glycol monobutyl ether (Butyl Carbitol™, ≥ 98 %; all sourced from Sigma-Aldrich, Steinheim, Germany) and 1-butanol (≥ 99.5 %, Merck, Darmstadt, Germany). Moreover, in order to make the dissolution results comparable with previous studies, the solubility of each lignin was also investigated in dimethyl sulfoxide (DMSO, ≥ 99.9 %, Sigma-Aldrich, Steinheim, Germany), the solvent commonly used for lignin dissolution.

2.2. Solubility of lignin in organic solvents

Two different methodologies (with minor modifications) were used for the dissolution experiments and these were based on details found in the literature (Cybulska et al., 2012; Shukry et al., 2008). Initially, solutions were prepared through the addition of a separate lignin sample (0.5 g) to a fixed volume of each organic solvent (25 mL) at room temperature. Solutions were then magnetically stirred (24 h), before being filtered (Paper #4, Whatman/GE Healthcare, China) and any insoluble remnants were dried at 50 °C for 24 h. In addition, for organic solvents that displayed high levels of lignin solubility (< 90 wt. %) the experiments were repeated with the same lignin concentrations (20 g/L) and any insoluble residues were separated by centrifugation at room temperature (5000 rpm, 10 min) using a ThermoFisher Scientific (Heraes Megafuge 16R, Osterode am Harz, Germany). Any insoluble materials present were oven-dried at 50 °C for 48 h and the solubility in each solvent was determined gravimetrically. Centrifugation experiments were conducted to eliminate the error arising from lignin adhesion to the filtration media and to ensure a precise comparison of solvating power for the most successful solvents.

2.3. Chemical composition of lignins

The ash content of lignins were determined by pyrolyzing them in a furnace (Nabertherm, Lilienthal, Germany) with a temperature of 525 °C for 4 h. The acid-soluble, acid-insoluble and carbohydrate content of the different lignin were determined via the NREL/TP-510-42618 analytical procedure (Sluiter et al., 2008). Briefly, each lignin sample (300 mg) was added to sulfuric acid (H_2SO_4, 72 %) and placed in a water bath (1 h, 30 °C). Following acidification, the lignin-acid mixtures were diluted with distilled water (84 mL) and hydrolyzing (1 h, 121 °C) in an autoclave (Systec D-23, Linden, Germany). Once hydrolysis was complete, the acid-insoluble lignin was separated from the soluble constituents using filtering crucibles (1G3, PYREX™, Thermo Fisher Scientific, USA), following overnight drying. Determination of acid soluble lignin from the filtrates was determined from the absorbance at a wavelength of 205 nm (Shimadzu UV-2550spectrophotometer, Kyoto, Japan) and carbohydrates in the filtrates were quantified by High Performance Anion Exchange Chromatography HPAE system (Dionex ICS-3000, California, USA), following the same procedure outlined in the NREL/TP-50-42618 (Sluiter et al., 2008) standard.

2.4. Determination of molecular weight by gel permeation chromatography (GPC)

In order to determine the average molecular weights for the lignin samples, alkaline aqueous phase gel permeation chromatography (GPC) was utilized. The analysis was conducted with an Agilent HPLC-system (1100series, Santa Clara, USA) by means of polymer standards service (PSS) columns (pore sizes of 100 Å, 500 Å, and 1000 Å), using a UV detector at 280 nm. NaOH with concentration of 0.1 M and a flow rate of 0.7 ml/min was used as an eluent. The total injection volume of each sample was 50 μl and at room temperature. The calibration curves were obtained with polystyrene sulfonate standards (ranging from 400 g/mol to 1000 g/mol and syringol 154 g/mol. The calculated molecular weight values were determined using Agilent OpenLab software.

2.5. Analysis of lignin with ^{31}P NMR and ^{13}C NMR

The content of hydroxyl groups of technical lignin samples was determined by ^{31}P-NMR, according to an optimized protocol previously described elsewhere (Balakshin and Capanema, 2015a). The solvent for preparation of samples and all the auxiliary solutions comprised of a mixture of pyridine and deuterated chloroform (1.6:1, v/v). Samples were prepared by complete dissolution of 40 mg of each lignin in 0.4 ml of this solvent mixture. In the next step, 50 µl of chromium (III) acetylacetonate solution (11.4 mg in 1 ml of the fresh solvent) and the required amount of internal standard (IS) solution (0.12 M endo-*n*-hydroxy-5-norbornene-2,3-dicarboximide) were added to the fresh solvent to obtain an IS/lignin ratio of 1:20 w/w. At the final stage, 100 µl of phosphorus-containing reagent (2-chloro-4,4,5,5-tetramethyl-1,3,2-dioxaphospholane) was added to the mixture and the vial content was vortexed prior to being transferred into an NMR tube for the measurement. NMR spectra were acquired by a Bruker Avance III 400 MHz spectrometer using 128 scans, with 1.0 s acquisition time and 5.0 s relaxation delay. The spectra were phased and calibrated using the signal of water-derivatized product (122.2 ppm).

The structure of lignin samples was further characterized by ^{13}C-NMR measurements following a previously described protocol (Balakshin and Capanema, 2015b). The analysis was carried out using a Bruker Avance 400 MHz Specrometer using a dedicated ^{13}C NMR probe device. In short, about 200 mg of each lignin was dissolved in 0.45 ml DMSO-d_6 containing a relaxation reagent chromium (III) acetylacetonate (6 mg/ml), and the internal standard (IS) trioxane (~40 mg/ml). The ratio of IS/lignin was adjusted to 1:10 wt/wt. For data acquisition, an inverse gate detection and a 90° pulse width, with a 1.1 s acquisition time and 2.0 relaxation delay were used. Furthermore, the spectra were recorded at 240-(-40) ppm interval, with approximate collection of 20 000 scans. The spectra were processed according to the aforementioned protocol (Balakshin and Capanema, 2015b).

2.6. Analysis of lignin with differential scanning calorimetry (DSC)

The determination of glass transition temperature (T_g) was obtained by DSC measurements (TA Instruments, DSC Q2000, New Castle, USA) for both technical lignins, as well as dried lignin after dissolution in solvents with high solubility levels ($<$ 90 wt. %). For the latter, highly concentrated solutions (100 g/l) were first dried on a watch glass (72 °C, 48 h) and removed from the surface after drying. For DSC measurements, the samples (6 − 7 mg) were placed in aluminum pans and were heated from 20 °C up to 200 °C (10 °C/min) and held at 200 °C for 10 min to eliminate any sample thermal history. In order to ensure measurement accuracy after the first stage, samples were cooled to 10 °C and then reheated to 200 °C at the same rate (10 °C/min). All the DSC measurements were conducted in a nitrogen (N_2) atmosphere. Glass transition temperatures (T_g) were obtained from the second heating cycle and were defined as the midpoint of the temperature range where changes to the heat capacity occurs.

2.7. Deposition of lignin coatings

In order to prepare the lignin coatings, high concentration (100 *g*/l) lignin solutions were prepared with strong industrial solvents, and any insoluble residues were separated by centrifugation. The resultant preparations were then applied by spray coating - using a conventional cup gun equipment (Satajet 20 B, Ludwigsberg, Germany) - on the surface of iron-phosphated steel panels (R-46-ICF, Q-lab, Ohio, USA), without any further modification of the metallic surface. Solutions were sprayed at comparative air pressures (~10^6 Pa), distances (~25 cm) and spray angles (~90°) relative to the surface of steel panels. The elemental composition of the steel panels used is outlined in Table 1 (Iron Phosphate Treatment, Q-LAB). Prior to deposition, the surface of each steel panel was wipe-cleaned with low lint tissues (Light-duty, VWR, Pennsylvania, USA) and ethanol (94.2 %, Altia, Rajamäki, Finland). After deposition, the wet thickness of coatings were measured using a wet film wheel (Elecometer 3230, Manchester, UK), following the ISO 2808-1B standard (EN ISO, 2017). Samples were subsequently left to dry at ambient temperature in a fume hood for 72 h before being cured in a pre-heated oven at 130 °C (Memert, UN30) for 30 min.

Table 1
Elemental composition of the utilized iron-phosphated steel panel (wt. %), as specified by the manufacturer (Iron Phosphate Treatment, Q-LAB).

Composition	Wt. %
C	< 0.15
P	< 0.03
S	< 0.035
Mn	< 0.6
Fe	Balance

2.8. Adhesion measurements of coatings and investigation of morphology

In order to investigate the adhesion of lignin coatings to iron-phosphated steel panels, a crosshatch cutter (Paint Test Equipment, Congleton, UK) was used, following the procedure of the ISO 2409 standard (EN ISO, 2013). In this method, a multiple blade cutter is applied normal to the surface of a coating and is followed by the application of an adhesive tape, which is then subsequently removed after 5 min at a specific angle of ~60°. The evaluation of the adhesion results was conducted by optical microscopy imaging (OM, Motic BA310Met-t, Xiamen, China). Additional microscopic observations were used to investigate the general condition of the dried coatings, as well as to image any plausible surface anomalies.

2.9. Investigation of electrochemical properties of lignin-coated steel panels

For investigation of the protection efficiencies against corrosion, linear sweep voltammetry (LSV) and electrochemical impedance spectroscopy (EIS) were used. All measurements were carried out using an Iviumstat XRe (Ivium Technologies, Eindhoven, The Netherlands) after exposure of samples to 250 ml of 5% NaCl solution in an Avesta cell with a fixed exposure area (0.785 cm^2). All the electrochemical measurements were conducted at room temperature using a three-electrode setup with a platinum (Pt) wire as the counter electrode (CE), Ag/AgCl (saturated KCl) as the reference electrode (RE) and the lignin-coated steel panels as the working electrode (WE). All electrochemical measurements were carried out after 1 h of stabilization of coatings in the electrolyte and were repeated in triplicate for each sample type.

Linear sweep voltammetry (LSV) diagrams were obtained at a scan rate of 0.5 mV/s and over a potential range of -0.4 to 0.4 V vs. open circuit potential (OCP) for individual samples. After each measurement, the current density (CD) value was determined from the linear region of the resulting Tafel diagram in proximal to the corrosion potential. The EIS measurements were performed under similar experimental conditions after an hour stabilization of WE in the electrolyte solution and over a frequency range of 50 kHz - 0.05 Hz. The frequency values were spaced logarithmically (10 steps per decade) with a voltage signal amplitude of 20 mV$_{rms}$ and at OCP values for each sample. The resulting EIS data was fitted using ZView® analysis software (Scribner Associates, North Carolina, USA).

3. Results and discussion

3.1. Solubility of lignin in organic solvents

Fig. 1 outlines the solubility of the two technical lignin samples in the organic solvents investigated as obtained by solid separation with filtration. Depending on the solvent, both lignin samples demonstrated partial to a near-complete solubility at the examined concentration (20 g/l), with the highest solubility percentages obtained for diethylene glycol monobutyl ether (Butyl Carbitol™, BC) and 1-methoxy-2-propanol (Dowanol™ PM, DPM), respectively. The solubility of lignins in both organic solvents were comparable with that of dimethyl sulfoxide (DMSO), which is generally considered to be a strong solvent for lignin

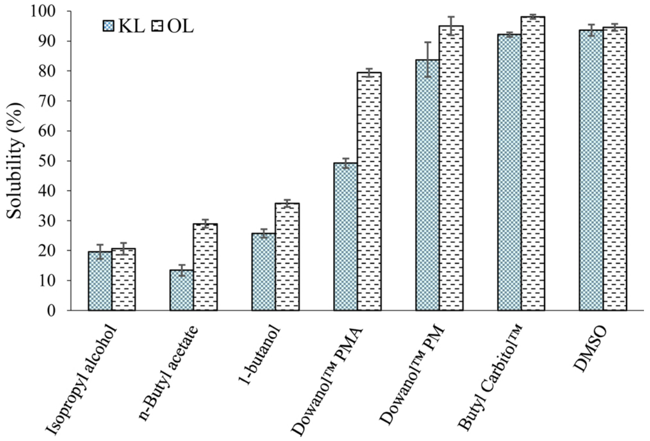

Fig. 1. Solubility (wt. %) of kraft lignin (KL, blue) and organosolv lignin (OL, Black) in organic solvents, obtained from filtration experiment.

Table 3
Hildebrand solubility parameter (δ_t), Hansen hydrogen bonding (δ_h) and polar interactions (δ_p) for the examined solvents. Values are arranged in order of ascending hydrogen bonding capabilities. All the values are adopted from Koleske and Hansen (2009), except Dowanol™ PMA (Dowanol™ PMA, Dow Chemicals).

No.	Solvent	δ_t[a]$(MPa)^{1/2}$	$\delta_p(MPa)^{1/2}$	δ_h $(MPa)^{1/2}$
1	n-Butyl acetate	17.4	3.7	6.3
2	Dowanol™ PMA	18.4	6.1	6.6
3	DMSO	26.7	16.4	10.2
4	Butyl Carbitol™ (BC)	20.4	7	10.6
5	Dowanol™ PM (DPM)	20.4	4.7	11.6
6	1-butanol	23.2	5.7	15.8
7	2-propanol	23.6	6.1	16.4

[a] Values are calculated based on the equation proposed by Koleske and Hansen (2009): $\delta_t^2 = \delta_d^2 + \delta_P^2 + \delta_h^2$.

(Duval et al., 2016). The other four industrial solvents demonstrated only a partial solubility of lignin, with higher dissolved quantities measured for organosolv lignin (OL) when compared to kraft lignin (KL) and this trend was consistent for all seven organic solvents examined.

In order to obtain more accurate results of solubility, centrifugation was used for solid-liquid separation (for BC, DPM, and DMSO), Table 2. From the results, it is clear that both OL and KL demonstrated the highest solubility in DMSO, closely followed by BC and then DPM. Furthermore, the trend for higher solubility of OL compared to KL in solvents was evident. Table 2 also lists the solubility values obtained from filtration experiments. The difference in solubility percentage amongst the two utilized solid-liquid separation techniques is probably a consequence of lignin adhesion to the filter paper.

As mentioned previously, the solubility parameters as defined by Hildebrand and Hansen theories help to explain the general solubility behavior of lignin in organic solvents. Table 3 summarizes the Hildebrand solubility parameter (δ_t) and Hansen solubility parameters related to hydrogen bonding (δ_h) and polar interactions (δ_p) (Koleske and Hansen, 2009). Schuerch (1952), has previously found that strong organic solvents for lignin are those with a solubility parameter close to 22.5 $(MPa)^{1/2}$ and that further increases in hydrogen bonding capability of these types of solvent results in enhanced lignin solubility. Based on these findings, solvents with solubility parameters close to the reported optimum value (No. 3 to 7 in Table 3) would be expected to demonstrate the highest levels of lignin solubility. Nevertheless, the pure alcohols - 1-butanol (No. 6) and 2-propanol (No. 7) - were determined to be the weakest solvents utilized in this study. This observation is probably due to the high level of association that occurs through hydrogen bonding with these types of alcohols, which leads to a decrease in the solubility power of the solvent (Duval et al., 2016; Koleske and Hansen, 2009). For the remaining solvents (No.3–5 in Table 3), the dissolved quantities of both KL and OL were the highest amongst the solvents investigated. Furthermore, the solvent power appeared to increase as the solvent's polarity increased from 4.7 $(MPa)^{1/2}$ for DPM, to 16.4 $(MPa)^{1/2}$ for DMSO. This is in agreement with the previous study of Duval et al. (2016), in which an increase in solvent polarity (δ_p) appeared to positively impact the solubility of kraft lignin (KL) in organic solvents. For Dowanol™ PMA, although the Hildebrand parameter (δ_t) and hydrogen bonding capabilities (δ_h) were lower than the other solvents (with the exception of n-butyl acetate), the solubility of lignin was relatively high, probably as a result of the polar interactions between the solvent and the solute. Nevertheless, the glycol ethers are generally considered to be strong solvents for lignin and it is therefore not surprising that the three best industrial solvents – Dowanol™ PM (DPM), Dowanol™ PMA, and Butyl Carbitol™ (BC) (Glycol Ethers, Dow Chemicals) – used in this study are based on such chemistry (Schuerch, 1952). It is worth noting however, that the parameters evaluated here definitively cannot alone elucidate the reasons for the higher observed solubility of OL when compared to KL.

3.2. Chemical composition of lignins

Table 4 lists the results of the Klason lignin and acid-soluble lignin tests, as well as moisture, ash and elemental sugars contents for KL and OL used in this study. As can be observed, there is a noticeable difference between the two lignin types as OL has a higher total lignin content of approx. 94 % - compared to 87 % for KL, smaller carbohydrate (monomeric residues) content of < 1% cf. ~6% for KL and significantly lower ash content (~0.1 % for OL compared to ~1% for KL). These findings demonstrate that the purity of OL is higher than KL, as would be expected from an organosolv production process (Pan, 2013). Consequently, the higher purity of OL could have contributed to its higher solubility in all the examined solvents when compared to KL; in fact, the content of monomeric residues from insoluble fraction of lignin

Table 2
Solubility of lignins in different organic solvents (wt. %), from centrifugation and filtration experiments.

Solvent	Solubility (wt. %) for KL		Solubility (wt. %) for OL	
	Centrifugation	Filtration	Centrifugation	Filtration
DMSO	99.9 (± 0.1)	93.7 (± 1.9)	100	94.6 (± 1.2)
BC	99.2 (± 0.2)	92.2 (± 0.8)	99.9 (± 0.1)	98.1 (± 0.7)
DPM	98.3 (± 0.3)	83.8 (± 5.8)	99.6 (± 0.2)	95.1 (± 3.1)
Dowanl™ PMA	NE	49.2 (± 1.6)	NE	79.4 (± 1.4)
1-butanol	NE	25.8 (± 1.4)	NE	35.8 (± 1.2)
n-Butyl acetate	NE	13.4 (± 1.8)	NE	29.0 (± 1.4)
2-propanol	NE	19.6 (± 2.4)	NE	20.6 (± 2.0)

NE: not examined.

Table 4
Chemical composition of kraft lignin (KL) and organosolv lignin (OL) (wt. % of lignin dry weight).

Constituent	KL	OL
Klason lignin	82.52 (± 0.29)	93.73 (± 0.22)
Acid-soluble lignin	4.46 (± 0.07)	1.72 (± 0.08)
Lignin (total)	86.98 (± 0.36)	95.45 (± 0.30)
Ash	0.92 (± 0.03)	0.13 (± 0.01)
Carbohydrate	6.23 (± 0.02)	0.90 (± 0.05)

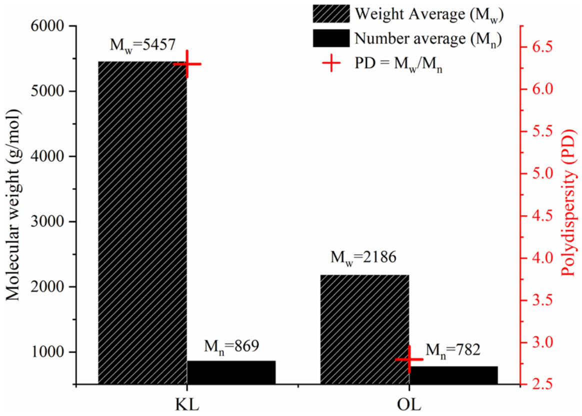

Fig. 2. The number average (Mn) and weight average (Mw) molecular weights, and polydispersity of (PD) of kraft lignin (KL) and organosolv lignin (OL).

is usually higher than those in soluble fractions (Duval et al., 2016; Robles et al., 2018; Ropponen et al., 2011).

3.3. Molecular weight measurements by gel permeation chromatography (GPC)

Fig. 2 shows the data obtained from the GPC measurements of KL and OL, including the number average (M_n) and weight average (M_w) molecular weights, as well as polydispersity (PS). The weight average molecular weight of kraft lignin (M_w = 5457 g/mol) is two times higher than that of organosolv lignin (M_w = 2186 g/mol). This distinct difference between two samples is most probably due to different nature of the source material, softwood vs. hardwood. It is known that softwood lignin is mainly composed of guaiacyl (G) units, while hardwood lignin contains both guaiacyl (G) and syringyl (S) units (Chen-Loung, 1991). As the presence of S units in hardwood structure inhibits the condensation reactions (Pan, 2013), its absence in softwood lignin results in more condensed structures and higher molecular weights (Baumberger et al., 2007; Glasser et al., 1993). In addition to the nature of lignin, the production process of samples could have contributed to the observed differences in molecular weights. In contrast to the kraft pulping process, which results in production of inherently heterogenous lignin with a high polydispersity index (Cui et al., 2014), the organosolv process yields lignin with relatively low molecular weight and a narrow polydispersity (Pan, 2013).

Another clear difference between the KL and OL is the higher index of PS in KL, which is an indication of the wider molecular weight distribution of KL (6.3) cf. OL (2.1) that also results from the kraft production process, as well as the presence of impurities in this sample. Therefore, the higher solubility of OL compared to KL lignin in all the solvents examined (aside from higher purity) can be postulated to the lower molecular weight and narrower weight distribution, which are both influential parameters for a higher solubility of lignin in organic solvents (Sameni et al., 2017; Schuerch, 1952). Furthermore, the higher degree of condensation in softwood KL can contribute to a lower degree of solubility in the examined solvents, as the diffusion of organic solvents into the structure - and therefore solubility (Pan and Sano, 1999) - is less than that of OL.

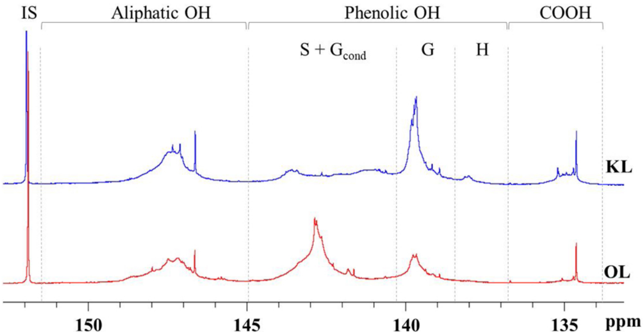

Fig. 3. Obtained ^{31}P NMR spectra for kraft lignin (KL, blue) and organosolv lignin (OL, black).

Table 5
Functional groups of softwood kraft lignin (KL) and hardwood organosolv lignin (OL), obtained by ^{31}P NMR (mmol/g lignin).

	KL	OL
S + G_{Cond} PhOH	1.94	2.66
$G_{non\text{-}cond}$ PhOH	2.00	1.00
H PhOH	0.32	NA
Total Phenolic	4.26	3.66
Aliphatic	2.27	1.79
COOH	0.62	0.21
Total OH	7.15	5.65

3.4. Determination of lignin functional groups by ^{31}P NMR and ^{13}C NMR

Fig. 3 displays the ^{31}P NMR spectra of both OL and KL, and Table 5 shows the number of hydroxyl groups in aliphatic, phenolic and carboxylic acid moieties. As expected, the amounts of 5-substituted PhOH is higher in OL, which arise from the contribution of S units. Furthermore, the amounts of total phenolic and aliphatic OH is slightly higher in the KL, 16 % and 26 % correspondingly, while the amount of COOH groups is 3 times higher than that of OL.

In general, lignin structures are very complex and contain various functional moieties, which affect the solubility of lignin in different organic solvents. However, the correlation between specific functional groups and solubility behavior is not necessarily clear. To elucidate this matter, comprehensive characterization of lignin structures is a necessity. Table 6 illustrates significant variations in the structural characteristics of analyzed lignins, obtained by ^{13}C NMR measurements. As expected, the amounts of methoxyl groups are higher in OL due to contribution of S units. Moreover, the more condensed structure of KL is also visible from this measurement. Furthermore, the presence of ethoxyl groups in OL structure are detected, which originate from the ethanol-based organosolv processing (Balakshin and Capanema, 2015b; Berlin et al., 2006). In addition, significant differences in carbonyl (CO) and carboxyl/ester groups (COOR), the amounts of protonated aromatic, as well as oxygenated and saturated aliphatic moieties are obvious (Table 6). KL also contains higher amounts of carbohydrates, which explains the lower solubility of KL compared to OL in solvents with lower polarities (Fig. 1, Section 3.1). However, the difference is very subtle when optimal solvents (DMSO, BC, and DPM) are used due to a high solubility of lignin at low concentration (2 wt. %) used in our experiments.

3.5. Determination of glass transition temperature (T_g) for technical lignin and dissolved samples

Fig. 4 presents the thermograms obtained from DSC measurements

Table 6
Structural characteristics of softwood kraft lignin (KL) and hardwood organosolv lignin (OL), obtained by ^{13}C NMR (per 100Ar and mmol/g lignin).

	KL		OL	
Moieties/range	per 100Ar	mmol/g	per 100Ar	mmol/g
Non-conjugated CO	6	0.35	9	0.48
Conjugated CO	4	0.23	11	0.59
Total CO	10	0.58	20	1.06
Non-conjugated COOR	16	0.92	9	0.48
Conjugated COOR	1	0.06	2	0.11
Total COOR	17	0.98	11	0.59
OMe	82	4.73	117	6.23
DC, %	76		44	
G_2	88	5.07	35	1.86
$S_{2,6}$	NA	NA	87	4.63
H (apprx.)	3	0.17	2	0.11
S + G + H	91	5.25	80.5	4.29
S/G ratio	NA		1.24	
ArH	221	12.75	184	9.80
Oxygen. Aliphatic	80	4.61	112	5.96
corrected for carbs	67	3.84		
Saturated Aliphatic	111	6.40	89	4.74
Side chain length	218		232	
corrected for carbs	178	10.24	NA	NA
β-O-4	5	0.29	7	0.37
Carbohydrates	3	0.17	< 1	
EtO-ether	NA	NA	9	0.48
EtO-ester	NA	NA	3	0.16
EtO-total	NA	NA	12	0.64
M_{Ar}	173		188	

NA: not applicable; DC: degree of condensation; M_{AR}: "molecular mass" values of an averaged lignin monomeric unit.

for KL (Fig. 4a) and OL (Fig. 4b) both as originally received and after resolidification following dissolution in organic solvents. For the technical lignin, it was observed that KL has a slightly higher T_g (151 °C) than OL (138.8 °C). These values are well within the range of reported T_g for technical lignins (90 − 180 °C) (Michelin et al., 2018). Moreover, the lower values obtained for OL (compared to KL) were in agreement with other works from the literature (Michelin et al., 2018; Sen et al., 2015). The T_g values obtained from DPM dissolutions demonstrated similar values (148.5 °C for KL and 137.4 °C for OL) with the original lignin samples, however, samples from the dissolution in BC demonstrated a significant decrease in their T_g values (~76 °C for KL and 81.2 °C for OL) probably as a result of plasticization induced by the solvent.

In general, plasticizers soften a polymer by increasing the free volume in the structure that results in a lower polymer T_g. Plasticizers either form a chemical bond with the polymer (internal plasticizers) or interact with the polymer by physical ingress in between the matrix chains, before gradually flowing from the polymeric matrix over time (external plasticizers). Organic solvents, especially those with a low vapor pressure, belong to the second category (Immergut And Mark, 1965). Considering the vapor pressure of these solvents (~4 Pa at 20 °C for BC and ~1100 Pa at 20 °C for DPM) (Glycol Ethers, Dow Chemicals), as well as the absence of any noticeable changes in the FTIR diagrams of the original lignin samples and re-solidified lignin after dissolution (Fig. S1, supporting information), it can be concluded that (unlike DPM) BC behaves as an external plasticizer for both KL and OL as it does not form a chemical bond with either. Therefore, the decreased T_g for lignin/BC samples suggest the presence of residual solvents in both lignin samples, which can influence the T_g values obtained from DSC measurements (Faris et al., 2017).

3.6. Deposition of coatings and investigation of adhesion and morphology

The deposition of coatings were conducted by spray application of dissolutions. The visual appearance of coated panels after 12 h from the application of dissolutions are displayed in Fig. S2 (supporting information). For lignin/DPM coatings, the surfaces appear relatively homogenous across the panels, whereas lignin/BC coatings show a variation in thickness across the panels and traces of solvent are visible in different regions on the surface. The thickness variation in lignin/BC results from the flow of dissolution - sagging - during the deposition and drying process. Such dissolution flow on a substrate is a well-known phenomenon for slow evaporating solvents like Butyl Carbitol™ (Stout, 2000).

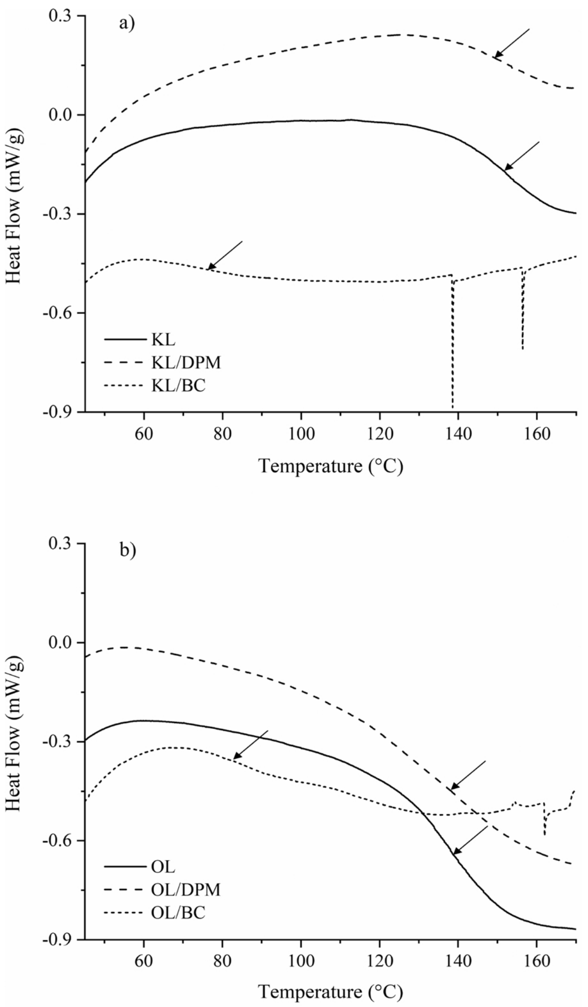

Fig. 4. DSC curves of KL (a) and OL (b), for the technical lignin (solid lines) and after solidification from DPM (dashed lines) and BC (dotted lines). The arrows indicate the glass transition temperature (T_g) for each sample.

An important requirement for a protective coating is its adhesion to the surface (Deflorian and Fedrizzi, 1999). Fig. 5 demonstrates the optical microscopy (OM) images, obtained after crosshatch adhesion measurements and from the intersection of the cuts on lignin coatings with wet thickness values of 6 − 8 μm, and Table 7 highlights the quantified adhesion values. As can be observed (Fig. 5), both KL and OL coatings that were prepared in BC demonstrate clear and well-defined edges in the cut area without any obvious separation/detachment of coatings from the surface (Fig. 5a and c). In contrast, coatings that were prepared from DPM (for both KL and OL) were slightly detached from the surface and in the vicinity of the cut lines for both KL (Fig. 5b) and OL (Fig. 5d) coatings, and thus demonstrated a weaker adhesion capabilities compared to lignin/BC coatings (Table 7). This behavior indicates that lignin/DPM coatings are somewhat more brittle than lignin/BC coatings, and notching of lignin/DPM coatings resulted in localized flaking of the coating adjacent to the cutting lines. This hypothesis is inline with DSC measurements, as lignin/BC coatings

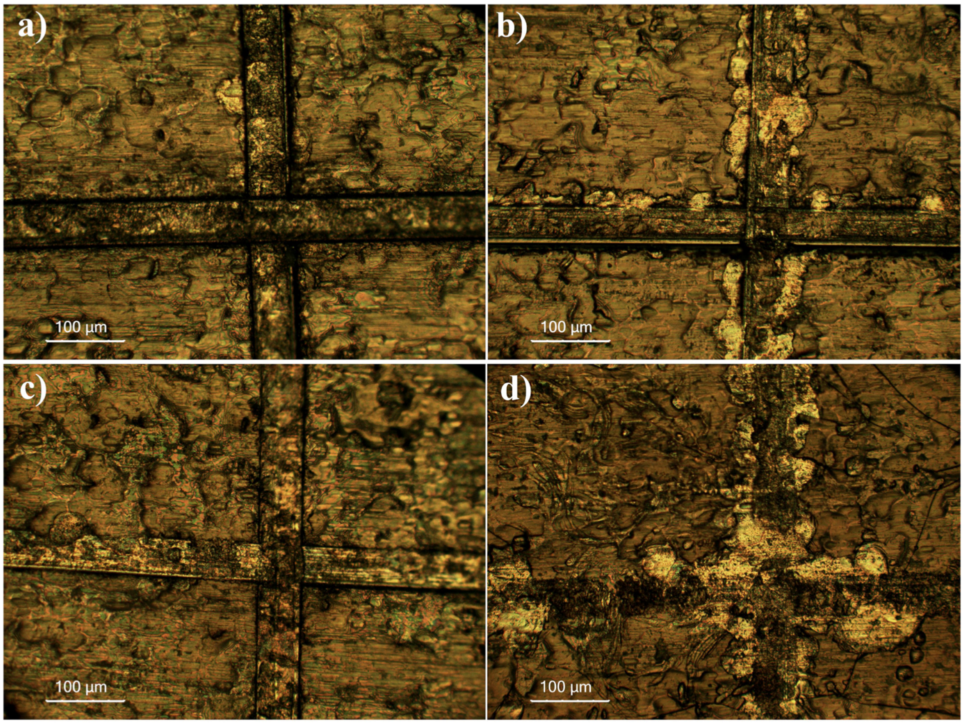

Fig. 5. Optical microscopy images of lignin coated surfaces after crosshatch adhesion measurements, for KL/BC (a), KL/DPM (b), OL/BC (c), and OL/DPM (d) (scale bar: 100 µm).

Table 7
Adhesion of lignin coatings from successful dissolution of KL and OL in two organic solvents. **N.B.** Based on ISO 2409 standard, adhesion values of 0 and 5 represent the best adhesion and the adhesion failure (> 65 % flaking of coatings), respectively (ISO 2409, 2013).

Solvent	Dowanol™ PM (DPM, 100 g/L)		Butyl Carbitol™ (BC, 100 g/L)	
Lignin sample	KL	OL	KL	OL
Adhesion value	1	2	0	0

demonstrate lower T_g values when compared to lignin/DPM coatings (Section 3.5.). However, the better adhesion performance of lignin/BC on steel may also result from differences in the substrate wetting properties of the organic solvents, which are known to be negatively affected by a fast evaporation rate (Stout, 2000). Nevertheless, these results signify that inherent differences in solvent properties - such as evaporation rate - have a critical impact on the adhesion performance of these types of lignin-based coatings.

The morphology of the lignin coatings was further investigated by optical microscopy and Fig. 6 clearly highlights the stressed nature of lignin/DPM coatings. For KL/DPM with initial wet thickness of 6 − 8 µm (Fig. 6a) the surface appears to be free of cracks, which changes to a surface with rather wide cracks when wet thickness is increased to 30 − 32 µm (Fig. 6b), whereas OL/DPM has a cracked surface irrespective of the initial wet thickness (Fig. 6c,d). It is clear from these results that an increase in coating thickness for both KL/DPM and OL/DPM enhances the extent of cracking. It must be noted that development of cracks in these coatings occurred prior to any heat treatment of the samples, which suggests that the origin of cracks does not result from any mismatch between the thermal expansion of the substrate and the lignin coatings. Nonetheless, for coatings that possessed initial cracks, the width of these cracks was observed to increase following heat-treatment. In contrast to lignin/DPM coatings, the surface of lignin/BC were found to be crack-free in all regions (Fig. S3, supporting information), including the positively sagged (thicker coatings) and the negatively sagged areas (thinner coatings).

Therefore, it is possible that the fast evaporation of solvent from lignin/DPM surfaces results in a constrained shrinkage that results in an accumulation of stress within the final dry coating (Francis et al., 2002). Another possibility is the external plasticization effect of the BC solvent on lignin, which results in a higher free volume within the matrix of the coating and as the amount of trapped solvents is smaller for polymers with a lower T_g – as shown by the related DSC measurements - a less constrained shrinkage of the coating occurs (Francis et al., 2002).

3.7. Electrochemical properties of lignin-coated steel surfaces

For investigation of anticorrosion properties of the coatings, KL/DPM and OL/DPM coatings with initial wet thickness values of 6 − 8 µm were selected for linear sweep voltammetry (LSV) measurements. Fig. 7 demonstrates the LSV diagrams and calculated current density (CD) values of the blank iron-phosphated steel as well as lignin/DPM coatings.

As shown in Fig. 7a, the coated surfaces resulted to a drop in current density (CD) values between 1–3 orders of magnitude, when compared to the uncoated steel surface. The lowest CD value (Fig. 7b), *i.e.* the highest protection against corrosion, amongst the coatings investigated was obtained with KL/ DPM, (2.5×10^{-8} A. cm^{-2}), followed by OL/DPM (2.8×10^{-7} A. cm^{-2}) cf. iron-phosphated steel (4.2×10^{-6} A. cm^{-2}). The higher CD value of the latter (thus a weaker protection) was expected as OL/DPM possessed a cracked surface, which was not the case for KL/DPM with a comparable wet thickness of 6 − 8 µm. Haro et al. (2019), have demonstrated that the CD values of a plasma-treated aluminum surface is comparable with that of a surface coated with unmodified softwood kraft lignin, which was thought to be due to weak adhesion between lignin and aluminum surface. In this case, however, both technical lignin sources used not only decrease CD, but also show acceptable levels of adhesion to the steel substrate surface.

The electrochemical performances of lignin/DPM coated samples were further investigated by electrochemical impedance spectroscopy (EIS) over a 24 h period of immersion in a 5% NaCl solution. Fig. 8

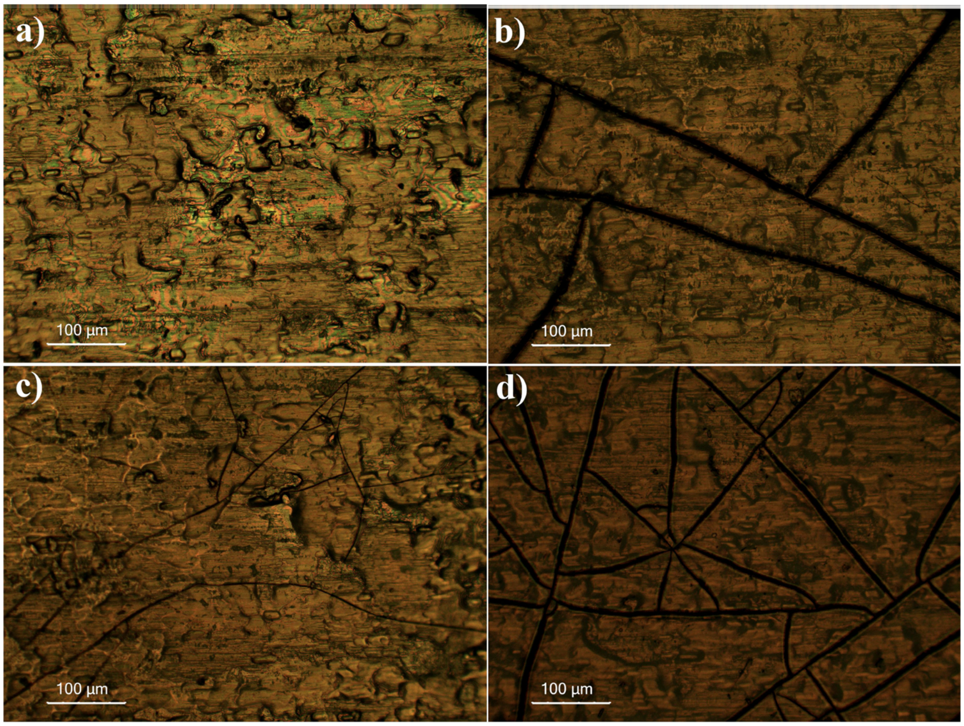

Fig. 6. Optical microscopy images of lignin/ DPM coatings with initial wet thickness values of 6-8 µm (a, c) and 30-32 µm (b, d) for KL (a, b) and OL (c, d) (scale bar: 100 µm).

outlines the Bode plots obtained from the lignin coatings and bare steel surfaces. In Bode plots of a corroding system, the low frequency plateau in the impedance modulus graph (Fig. 8a) represents the charge transfer resistance (R_{ct}) at the interface of coating and the corroding metal and can be related to the degree of protection provided by the coating (Kumar and Buchheit, 2006; Oliveira and Ferreira, 2003a). By comparing the low frequency impedance values obtained from the steel and coated surfaces, it can be seen that both the KL/DPM and OL/DPM coatings provide barrier properties after 1 h of immersion in the electrolyte, with a greater charge transfer resistance evident for KL/DPM. After 24 h immersion, the OL/DPM coating appears to no longer provide any protection against the corrosion and the coating was found to have almost completely degraded (as shown in Fig. S4a, supporting information). In contrast, the KL/DPM coating is able to maintain a level protection throughout the 24 h timeframe, although the protection performance is observed to decrease. Furthermore, evidence of pitting corrosion can be seen in KL/DPM coated steel in the form of an uneven distribution of pitting on the surface of the underlying steel (Fig. S4b and c) after 1 day of immersion in the 5% NaCl solution.

Another criterion for evaluation of EIS data is to compare the theta values obtained from the related Bode phase angle plots (Fig. 8b). In theory, the theta values at high frequency (10^4 Hz) for a coated metal (capacitor and resistor in parallel) should be close to 90° values if the current passes through the capacitor or almost 0° if the current mostly passes through the resistor. In the case of the coated samples of this study, it can be seen that both KL/DPM and OL/DPM samples demonstrate capacitive-dominant behavior at high frequencies (with a more dominant capacitive behavior for KL/DPM compared to OL/DPM) and that the theta values are notably higher than that of the uncoated iron-phosphated steel. Nevertheless, with prolonged immersion, theta values for both coatings are reduced to levels similar to that of the bare metal, which indicates that both lignin-based coatings undergo some form of degradation with extended exposure to such an aggressive electrolyte (Mahdavian and Attar, 2006).

The lower barrier performance of OL/DPM recorded can be explained by the cracked texture of the coating that exposes the underlying steel surface and allows higher levels of metal dissolution. In addition, the Bode plots also highlight that neither of the two coatings demonstrate a purely capacitive behavior, which comprises of a straight line with a 45° angle over the scan frequency range (Duval et al., 2000). A comparison of the Bode plots outlined here with the results from our previous study - in which a near-ideal capacitive behavior was observed in Bode plots of spin-coated organosolv lignin coatings (Dastpak et al., 2018) - it can be clearly demonstrated that not only the source of lignin but also the deposition method has major influence on the resultant lignin coating performance. Unlike spin coating, which is known to produce a highly uniform surface layer (Norrman et al., 2005), deposition of a thin lignin layer by an industrial painting method like spraying might not necessarily provide a uniform and defect-free coating, therefore any pathways for electrolyte ingress would tend to be short as result of the low level of coating thickness (Oliveira and Ferreira, 2003b).

The experimental EIS data were quantified using equivalent circuits (ECs), which are shown in Fig. 9. In these circuits, R represent the resistive elements and CPE the constant phase element that exemplifies any non-ideal capacitive behavior. In these circuits, R_S is the solution resistance and each coating layer consists of a resistance that is paired with a parallel capacitance as the system is comprised of a phosphate-treatment layer (R_O and CPE_O) and the lignin coating (R_C and CPE_C). Furthermore, upon ingress of electrolyte into the coatings and to the innermost interface, i.e. oxide/steel interface, the charge transfer resistance (R_{ct}) and capacitance of the electric double layer (CPE_{dl}) are utilized to reflect the electrochemical reactions at this interface. For the cracked OL/DPM coatings, a Warburg element (W) is included in the EC to reflect the mass transport of electroactive moieties at the lowest scan frequencies (Fernández-Sánchez et al., 2005), as shown in Nyquist plot of OL/DPM after 1 h immersion (Figure S5, Supporting Information). The results from the fitting of EIS data with the different ECs are listed in Table S1 (Supporting Information).

The charge transfer resistance of the coatings of this study are listed (Table 8) alongside other corrosion resistant coatings based either partially or completely on renewable feedstocks previously reported.

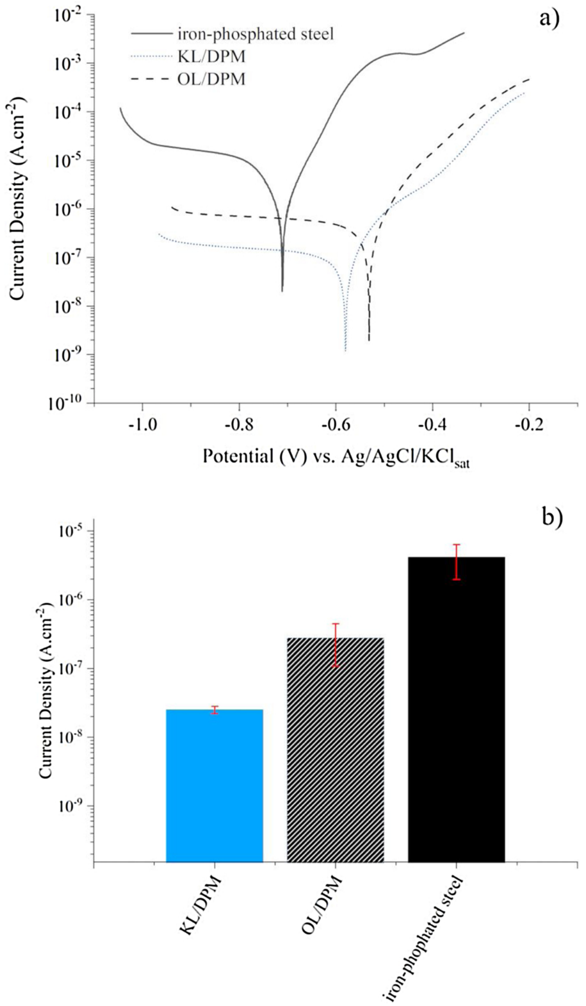

Fig. 7. Linear sweep voltammograms of bare iron-phosphated steel and lignin-coated surfaces, after 1 h immersion in 5% NaCl (sweep rate: 0.5 mV.s^{-1}) (a) and calculated values of current densities (CDs) from LSV measurements of the samples (b). **N.B.** smaller CD values represent a higher corrosion protection performance.

The higher R_{ct} values of KL/DPM after both 1 -h immersion (1.5×10^5 $\Omega.\,cm^2$) and 24 h of immersion (1.1×10^4 $\Omega.\,cm^2$) are higher than that of the bare steel (1.9×10^3 $\Omega.\,cm^2$), which demonstrate the anticorrosive capability of this coating system. Furthermore, the R_{ct} values of the lignin coatings, specifically KL/DPM, are comparable with other reported corrosion resistant coatings, although the coatings of this study had low thicknesses and were not cross-linked with any performance-enhancing organic/inorganic components.

4. Conclusions

Driven by the sustainability aspects of increasing the proportion of renewable materials in coatings, the current study demonstrates a straightforward route for preparation of lignin-based anticorrosive coating. Six different organic solvents were investigated as potential solvents of lignin, and consequently two industrially utilized organic solvents, i.e. Dowanol™ PM and Butyl Carbitol™ were shown to be successful. Both lignins (OL and KL) investigated demonstrated a high solubility, regardless of the fact that they hold a big difference in the content of functional groups and the average molecular weight values. It was shown that a thin layer of spray-coated kraft lignin from dissolution in Dowanol™ PM, had the capability to decrease the current density of iron-phosphated steel for more than two orders of magnitude (from 4.2×10^{-6} A. cm^{-2} for iron-phosphated steel vs. 2.5×10^{-8} A. cm^{-2} coated surfaces) and to increase the charge transfer resistance (Rct) of the steel from 1.9×10^3 $\Omega.\,cm^2$ to 1.5×10^5 $\Omega.\,cm^2$. The charge transfer resistance of the coating after 24 h immersion to 5% NaCl was still higher than that of the steel sample, even though some degradation of the coating was observed. The resultant solvent-based solutions can subsequently be utilized to produce a spray-coated

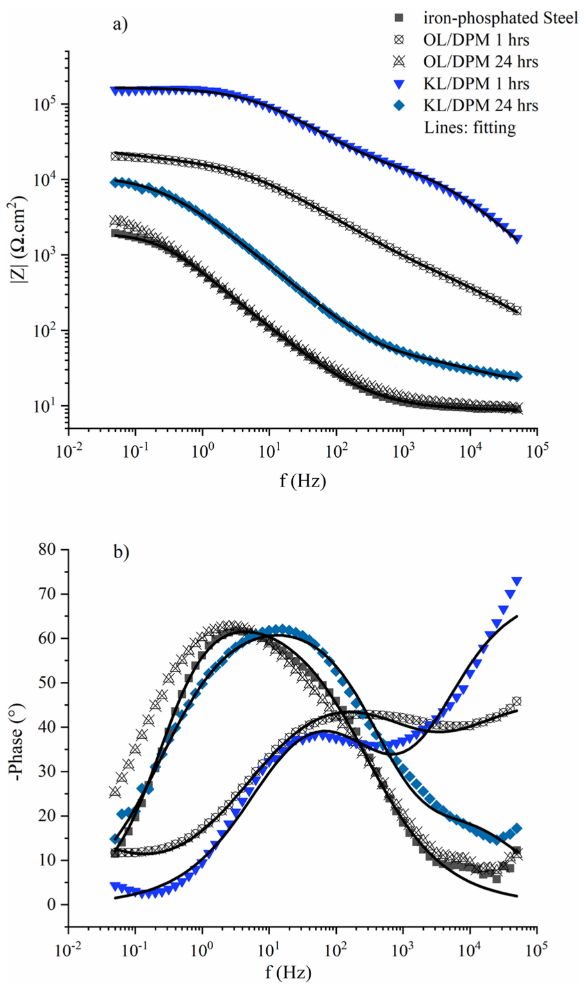

Fig. 8. Bode plots of bare iron-phosphated steel and lignin-coated surfaces, after 1 and 24 h immersion in 5% NaCl: a) impedance modulus vs. frequency, b) phase angle vs. frequncy. The solid lines represent the simulated data from fitting with equivalent circuits.

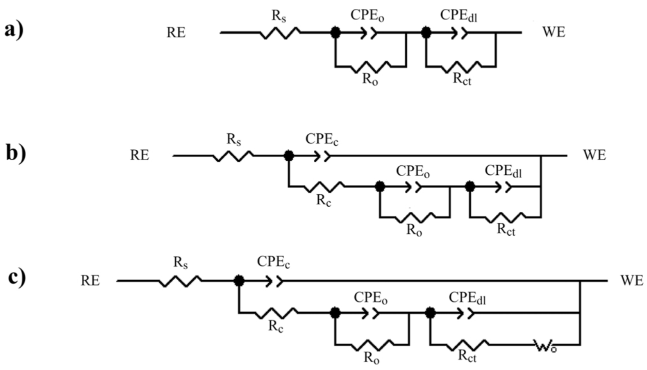

Fig. 9. Equivalent circuits (ECs) utilized for fitting the EIS data for the bare iron-phosphated steel (a), KL/DPM (b), and OL/DPM (c) after immersion in 5% NaCl. RE stands for reference electrode and WE for working electrode.

Table 8
Comparison of R_{ct} values from the coating system used in this work and other reported studies based on partial/complete renewable feedstocks.

Coating system	Substrate	Medium	R_{ct} (Ω. cm^2) coated vs. bare substrate	Reference No.
KL/DPM after 1 hour immersion	iron-phosphated steel	5% NaCl	1.5×10^5vs.1.9×10^3	This study
KL/DPM after 24 hours immersion	iron-phosphated steel	5% NaCl	1.1×10^4vs.1.9×10^3	
Water-based polyurethane dispersion with lignosulfonate-modified ZnO nanoparticles	mild steel	3.5 % NaCl	3.7×10^3vs.2.0×10^2	(Christopher et al., 2016)
Multilayer chitosan/diclofenac coatings, after 10 hours immersion	stainless steel 316 LVM	0.9 % NaCl	2.3×10^3vs.1.5×10^3	(Finšgar et al., 2016)
Multilayer coatings of cross-linked chitosan and poly(vinyl butyral) after 24 hours immersion	carbon steel	0.3 M salt solution	8.9×10^5	(Luckachan and Mittal, 2015)
Chitosan cross-linked with glutaraldehyde	mild steel	0.5 M H_2SO_4	1.3×10^2vs.4.5×10^1	(Ahmed et al., 2012)

surfaces that has good to excellent adhesion characteristics (ISO 2409, grades 0 and 1) and offers enhanced levels of corrosion behavior in relatively aggressive media (5% NaCl). Nevertheless, prolonged exposure times (> 24 h) may challenge continued performance and is a subject for further investigations.

CRediT authorship contribution statement

Arman Dastpak: Methodology, Formal analysis, Investigation, Data curation, Writing - original draft, Writing - review & editing, Visualization. **Tainise V. Lourençon:** Formal analysis, Investigation, Data curation, Writing - original draft, Writing - review & editing. **Mikhail Balakshin:** Investigation, Data curation, Writing - original draft, Writing - review & editing. **Syed Farhan Hashmi:** Formal analysis, Investigation, Data curation, Writing - review & editing. **Mari Lundström:** Conceptualization, Methodology, Validation, Formal analysis, Resources, Writing - review & editing, Supervision, Project administration, Funding acquisition. **Benjamin P. Wilson:** Conceptualization, Methodology, Validation, Resources, Writing - review & editing, Supervision, Project administration, Funding acquisition.

Declaration of Competing Interest

The authors declare that they have no known competing financial interests or personal relationships that could have appeared to influence the work reported in this paper.

Acknowledgements

This research was funded by Technology Industries of Finland/Jane and Aatos Erkko Foundations “Future Makers: Biorefinery Side Stream Materials for Advanced Biopolymer Materials (BioPolyMet)” and Academy of Finland NoWASTE, No. 297,962. Furthermore, this work utilized facilities provided by the RawMatTERS Finland Infrastructure RAMI at Aalto University, supported by the Academy of Finland. Additionally, special thanks to Antti Karkola and Marja Juvonen (Teknos Group Oy) for sharing expertise and providing metallic panels, Dr. Moritz Leschinsky (Fraunhofer Center for Chemical-Biotechnological Processes (CBP)) for providing the organosolv lignin, and Rita Hatakka for assistance with the chemical composition analysis of the lignins.

Appendix A. Supplementary data

Supplementary material related to this article can be found, in the online version, at doi:https://doi.org/10.1016/j.indcrop.2020.112310.

References

Abu-Dalo, M.A., Al-Rawashdeh, N.A.F., Ababneh, A., 2013. Evaluating the performance of sulfonated Kraft lignin agent as corrosion inhibitor for iron-based materials in water distribution systems. Desalination. https://doi.org/10.1016/j.desal.2012.12.007.

Ahmed, R.A., Farghali, R.A., Fekry, A.M., 2012. Study for the stability and corrosion inhibition of electrophoretic deposited chitosan on mild steel alloy in acidic medium. Int. J. Electrochem. Sci. 7, 7270–7282.

Akbarzadeh, E., Ibrahim, M.N.M., Rahim, A.A., 2011. Corrosion inhibition of mild steel in near neutral solution by Kraft and Soda lignins extracted from oil palm empty fruit bunch. Int. J. Electrochem. Sci. 6, 5396–5416.

Balakshin, M., Capanema, E., 2015a. On the quantification of lignin hydroxyl groups with ^{31}P and ^{13}C NMR spectroscopy. J. Wood Chem. Technol. https://doi.org/10.1080/02773813.2014.928328.

Balakshin, M.Y., Capanema, E.A., 2015b. Comprehensive structural analysis of biorefinery lignins with a quantitative ^{13}C NMR approach. RSC Adv. https://doi.org/10.1039/c5ra16649g.

Baumberger, S., Abaecherli, A., Fasching, M., Gellerstedt, G., Gosselink, R., Hortling, B., Li, J., Saake, B., De Jong, E., 2007. Molar mass determination of lignins by size-exclusion chromatography: towards standardisation of the method. Holzforschung. https://doi.org/10.1515/HF.2007.074.

Berlin, A., Balakshin, M., 2014. Industrial lignins. Bioenergy Research: Advances and Applications. Elsevier, pp. 315–336. https://doi.org/10.1016/B978-0-444-59561-4.00018-8.

Berlin, A., Balakshin, M., Gilkes, N., Kadla, J., Maximenko, V., Kubo, S., Saddler, J., 2006. Inhibition of cellulase, xylanase and β-glucosidase activities by softwood lignin preparations. J. Biotechnol. https://doi.org/10.1134/S0965545X06020155.

Chen-Loung, C., 1991. Lignins: occurrence in woody tissues, isolation, reactions, and structure. Wood Structure and Composition. Marcel Dekker, New York, pp. 183–261.

Christopher, G., Kulandainathan, M.A., Harichandran, G., 2016. Biopolymers nanocomposite for material protection: Enhancement of corrosion protection using waterborne polyurethane nanocomposite coatings. Prog. Org. Coatings. https://doi.org/10.1016/j.porgcoat.2016.05.012.

Cui, C., Sun, R., Argyropoulos, D.S., 2014. Fractional precipitation of softwood kraft lignin: isolation of narrow fractions comon to a variety of lignins. ACS Sustain. Chem. Eng. https://doi.org/10.1021/sc400545d.

Cybulska, I., Brudecki, G., Rosentrater, K., Julson, J.L., Lei, H., 2012. Comparative study of organosolv lignin extracted from prairie cordgrass, switchgrass and corn stover. Bioresour. Technol. https://doi.org/10.1016/j.biortech.2012.05.073.

Dastpak, A., Yliniemi, K., de Oliveira Monteiro, M., Höhn, S., Virtanen, S., Lundström, M., Wilson, B., 2018. From waste to valuable resource: lignin as a sustainable anti-corrosion coating. Coatings. https://doi.org/10.3390/coatings8120454.

Deflorian, F., Fedrizzi, L., 1999. Adhesion characterization of protective organic coatings by electrochemical impedance spectroscopy. J. Adhes. Sci. Technol. https://doi.org/10.1163/156856199X00154.

Ding, J., Gu, L., Dong, W., Yu, H., 2016. Epoxidation modification of renewable lignin to improve the corrosion performance of epoxy coating. Int. J. Electrochem. Sci. https://doi.org/10.20964/2016.07.56.

Duval, S., Camberlin, Y., Glotin, M., Keddam, M., Ropital, F., Takenouti, H., 2000. Characterization of organic coatings in sour media and influence of polymer structure on corrosion performance. Prog. Org. Coatings. https://doi.org/10.1016/S0300-9440(00)00094-1.

Duval, A., Vilaplana, F., Crestini, C., Lawoko, M., 2016. Solvent screening for the fractionation of industrial kraft lignin. Holzforschung. https://doi.org/10.1515/hf-2014-0346.

EN ISO, 2013. 2409: 2013 Paints and Varnishes — Cross-cut Test. ISO: Geneva, Switzerland.

EN ISO, 2017. 2808:2017 Paints and Varnishes — Determination of Film Thickness. ISO: Geneva, Switzerland.

Evstigneev, E.I., 2010. Specific features of lignin dissolution in aqueous and aqueous-organic media. Russ. J. Appl. Chem. https://doi.org/10.1134/S1070427210030250.

Faris, A.H., Rahim, A.A., Mohamad Ibrahim, M.N., Hussin, M.H., Alkurdi, A.M., Salehabadi, A., 2017. Investigation of oil palm based Kraft and auto-catalyzed organosolv lignin susceptibility as a green wood adhesives. Int. J. Adhes. Adhes. https://doi.org/10.1016/j.ijadhadh.2017.01.006.

Fernandes, E.M., Pires, R.A., Mano, J.F., Reis, R.L., 2013. Bionanocomposites from lignocellulosic resources: properties, applications and future trends for their use in the biomedical field. Prog. Polym. Sci. https://doi.org/10.1016/j.progpolymsci.2013.05.013.

Fernández-Sánchez, C., McNeil, C.J., Rawson, K., 2005. Electrochemical impedance spectroscopy studies of polymer degradation: application to biosensor development. TrAC - Trends Anal. Chem. https://doi.org/10.1016/j.trac.2004.08.010.

Finšgar, M., Uzunalić, A.P., Stergar, J., Gradišnik, L., Maver, U., 2016. Novel chitosan/

diclofenac coatings on medical grade stainless steel for hip replacement applications. Sci. Rep. https://doi.org/10.1038/srep26653.

Francis, L.F., McCormick, A.V., Vaessen, D.M., Payne, J.A., 2002. Development and measurement of stress in polymer coatings. J. Mater. Sci. https://doi.org/10.1023/A:1020886802632.

Giummarella, N., Lindgren, C., Lindström, M.E., Henriksson, G., 2016. Lignin prepared by ultrafiltration of black liquor: investigation of solubility, viscosity, and ash content. BioResources. https://doi.org/10.15376/biores.11.2.3494-3510.

Glasser, W.G., 1999. Classification of lignin according to chemical and molecular structure. In: Lignin: Historical, Biological, and Materials Perspectives, ACS Symposium Series. American Chemical Society. pp. 216–238. https://doi.org/10.1021/bk-2000-0742.ch009. SE–9.

Glasser, W.G., Davé, V., Frazier, C.E., 1993. Molecular weight distribution of (semi-) commercial lignin derivatives. J. Wood Chem. Technol. https://doi.org/10.1080/02773819308020533.

Hämäläinen, V., Grönroos, T., Suonpää, A., Heikkilä, M.W., Romein, B., Ihalainen, P., Malandra, S., Birikh, K.R., 2018. Enzymatic processes to unlock the lignin value. Front. Bioeng. Biotechnol. https://doi.org/10.3389/fbioe.2018.00020.

Harb, S.V., Cerrutti, B.M., Pulcinelli, S.H., Santilli, C.V., Hammer, P., 2015. Siloxane-PMMA hybrid anti-corrosion coatings reinforced by lignin. Surf. Coatings Technol. https://doi.org/10.1016/j.surfcoat.2015.05.002.

Holladay, J., Bozell, J., White, J., Johnson, D., 2007. Top Value Added Chemicals from Biomass - Volume II, Results of Screening for Potential Candidates from Biorefinery Lignin. Pacific Northwest National Library, United States. https://doi.org/10.2172/921839.

Hussin, M.H., Rahim, A.A., Mohamad Ibrahim, M.N., Brosse, N., 2015a. Improved corrosion inhibition of mild steel by chemically modified lignin polymers from Elaeis guineensis agricultural waste. Mater. Chem. Phys. https://doi.org/10.1016/j.matchemphys.2015.07.030.

Hussin, M.H., Shah, A.M., Rahim, A.A., Ibrahim, M.N.M., Perrin, D., Brosse, N., 2015b. Antioxidant and anticorrosive properties of oil palm frond lignins extracted with different techniques. Ann. For. Sci. https://doi.org/10.1007/s13595-014-0405-1.

Immergut, E.H., Mark, H.F., 1965. Principles of Plasticization. https://doi.org/10.1021/ba-1965-0048.ch001.

Koleske, J., Hansen, C., 2009. Chapter 35—Solubility parameters. Paint and Coating Testing Manual, Fourteenth Edition of the Gardner-Sward Handbook. https://doi.org/10.1520/mnl10214m.

Kumar, G., Buchheit, R.G., 2006. Development and characterization of corrosion resistant coatings using natural biopolymer chitosan. ECS Transactions. https://doi.org/10.1149/1.2215582.

Laurichesse, S., Avérous, L., 2014. Chemical modification of lignins: towards biobased polymers. Prog. Polym. Sci. https://doi.org/10.1016/j.progpolymsci.2013.11.004.

Lora, J.H., Glasser, W.G., 2002. Recent industrial applications of lignin: a sustainable alternative to nonrenewable materials. J. Polym. Environ. https://doi.org/10.1023/A:1021070006895.

Luckachan, G.E., Mittal, V., 2015. Anti-corrosion behavior of layer by layer coatings of cross-linked chitosan and poly(vinyl butyral) on carbon steel. Cellulose. https://doi.org/10.1007/s10570-015-0711-2.

Mahdavian, M., Attar, M.M., 2006. Another approach in analysis of paint coatings with EIS measurement: phase angle at high frequencies. Corros. Sci. https://doi.org/10.1016/j.corsci.2006.03.012.

Melro, E., Alves, L., Antunes, F.E., Medronho, B., 2018. A brief overview on lignin dissolution. J. Mol. Liq. https://doi.org/10.1016/j.molliq.2018.06.021.

Michelin, M., Liebentritt, S., Vicente, A.A., Teixeira, J.A., 2018. Lignin from an integrated process consisting of liquid hot water and ethanol organosolv: physicochemical and antioxidant properties. Int. J. Biol. Macromol. https://doi.org/10.1016/j.ijbiomac.2018.08.046.

Miller-Chou, B.A., Koenig, J.L., 2003. A review of polymer dissolution. Prog. Polym. Sci. https://doi.org/10.1016/S0079-6700(03)00045-5.

Norrman, K., Ghanbari-Siahkali, A., Larsen, N.B., 2005. Studies of spin-coated polymer films. Annu. Reports Prog. Chem. - Sect. C. https://doi.org/10.1039/b408857n.

Oliveira, C.G., Ferreira, M.G.S., 2003a. Ranking high-quality paint systems using EIS. Part II: defective coatings. Corros. Sci. https://doi.org/10.1016/S0010-938X(02)00089-6.

Oliveira, C.G., Ferreira, M.G.S., 2003b. Ranking high-quality paint systems using EIS. Part I: intact coatings. Corros. Sci. https://doi.org/10.1016/S0010-938X(02)00088-4.

Pan, X., 2013. Organosolv biorefining platform for producing chemicals, fuels, and materials from lignocellulose. In: Xie, H., Gathergood, N. (Eds.), The Role of Green Chemistry in Biomass Processing and Conversion. John Wiley & Sons Inc., pp. 241–262 Ebook ISBN: 9781118449424.

Pan, X.J., Sano, Y., 1999. Atmospheric acetic acid pulping of rice straw IV: physico-chemical characterization of acetic acid lignins from rice straw and woods. Part 2. Chemical structures. Holzforschung. https://doi.org/10.1515/HF.1999.098.

Ragauskas, A.J., Beckham, G.T., Biddy, M.J., Chandra, R., Chen, F., Davis, M.F., Davison, B.H., Dixon, R.A., Gilna, P., Keller, M., Langan, P., Naskar, A.K., Saddler, J.N., Tschaplinski, T.J., Tuskan, G.A., Wyman, C.E., 2014. Lignin valorization: improving lignin processing in the biorefinery. Science. https://doi.org/10.1126/science.1246843.

Rahman, O.U., Shi, S., Ding, J., Wang, D., Ahmad, S., Yu, H., 2018. Lignin nanoparticles: synthesis, characterization and corrosion protection performance. New J. Chem. https://doi.org/10.1039/c7nj04103a.

Ralph, J., Lundquist, K., Brunow, G., Lu, F., Kim, H., Schatz, P.F., Marita, J.M., Hatfield, R.D., Ralph, S.A., Christensen, J.H., Boerjan, W., 2004. Lignins: natural polymers from oxidative coupling of 4-hydroxyphenyl- propanoids. Phytochem. Rev. https://doi.org/10.1023/B:PHYT.0000047809.65444.a4.

Ren, Y., Luo, Y., Zhang, K., Zhu, G., Tan, X., 2008. Lignin terpolymer for corrosion inhibition of mild steel in 10% hydrochloric acid medium. Corros. Sci. https://doi.org/10.1016/j.corsci.2008.08.019.

Robles, J.D., Tamminen, T., Liitiä, T., Peresin, M.S., Rodríguez, A., Jääskeläinen, A.S., 2018. Aqueous acetone fractionation of kraft, organosolv and solda lignins. Int. J. Biol. Macromol. https://doi.org/10.1016/j.ijbiomac.2017.08.102.

Ropponen, J., Räsänen, L., Rovio, S., Ohra-aho, T., Liitiä, T., Mikkonen, H., Pas, D., Tamminen, T., 2011. Solvent extraction as a means of preparing homogeneous lignin fractions. Holzforschung. https://doi.org/10.1515/hf.2011.089.

Rossberg, C., Leschinsky, M., Janzon, R., Saake, B., 2019. Effect of process parameters in pilot scale operation on properties of Organosolv lignin. BioResources. https://doi.org/10.15376/biores.14.2.4543-4559.

Sakhri, A., Perrin, F.X., Benaboura, A., Aragon, E., Lamouri, S., 2011. Corrosion protection of steel by sulfo-doped polyaniline-pigmented coating. Prog. Org. Coatings. https://doi.org/10.1016/j.porgcoat.2011.06.005.

Sameni, J., Krigstin, S., Sain, M., 2017. Solubility of lignin and acetylated lignin in organic solvents. BioResources. https://doi.org/10.15376/biores.12.1.1548-1565.

Schuerch, C., 1952. The Solvent Properties of Liquids and Their Relation to the Solubility, Swelling, Isolation and Fractionation of Lignin. J. Am. Chem. Soc. https://doi.org/10.1021/ja01140a020.

Sen, S., Patil, S., Argyropoulos, D.S., 2015. Thermal properties of lignin in copolymers, blends, and composites: a review. Green Chem. https://doi.org/10.1039/c5gc01066g.

Shivakumar, M., Dharmaprakash, M.S., Manjappa, S., Nagashree, K.L., 2017. Corrosion inhibition performance of lignin extracted from black liquor on mild steel in 0.5 m H2SO4 acidic media. Port. Electrochim. Acta. https://doi.org/10.4152/pea.201706351.

Shukry, N., Fadel, S.M., Agblevor, F.A., El-Kalyoubi, S.F., 2008. Some physical properties of acetosolv lignins from bagasse. J. Appl. Polym. Sci. https://doi.org/10.1002/app.28059.

Sluiter, A., Hames, B., Ruiz, R., Scarlata, C., Sluiter, J., Templeton, D., Crocker, D., 2008. Determination of Structural Carbohydrates and Lignin in Biomass. National Renewable Energy Laboratory (NREL), United States.

Stout, R.L., 2000. Solvents in today's coatings. Applied Polymer Science: 21st Century. https://doi.org/10.1016/b978-008043417-9/50030-1.

Thakur, V.K., Thakur, M.K., Raghavan, P., Kessler, M.R., 2014. Progress in green polymer composites from lignin for multifunctional applications: a review. ACS Sustain. Chem. Eng. https://doi.org/10.1021/sc500087z.

References

Upton, B.M., Kasko, A.M., 2016. Strategies for the conversion of lignin to high-value polymeric materials: review and perspective. Chem. Rev. https://doi.org/10.1021/acs.chemrev.5b00345.

Vagin, M.Y., Trashin, S.A., Karyakin, A.A., 2006. Corrosion protection of steel by electropolymerized lignins. Electrochem. Commun. https://doi.org/10.1016/j.elecom.2005.10.023.

Xue, Z., Zhao, X., Sun, R.C., Mu, T., 2016. Biomass-derived γ-valerolactone-based solvent systems for highly efficient dissolution of various lignins: Dissolution behavior and mechanism study. ACS Sustain. Chem. Eng. https://doi.org/10.1021/acssuschemeng.6b00639.